# Supporting Information (SI) Appendix

*Title*: **Biodegradable Piezoelectric Force Sensor**

*Eli J. Curry[1], Kai Ke[2], Meysam T. Chorsi[2], Kinga S. Wrobel[2], Albert N. Miller III[2], Avi Patel[3], Insoo Kim[1,4], Jianlin Feng[5], Lixia Yue[5], Qian Wu[6], Chia-Ling Kuo[7], Kevin W.-H. Lo[1,8,9], Cato T. Laurencin[1,9,10], Horea Ilies[2], Prashant K. Purohit[11], Thanh D. Nguyen,[1,2,9]*

[1] Department of Biomedical Engineering, UCONN,
260 Glenbrook Road, Storrs, CT 06269, United States
[2] Department of Mechanical Engineering, UCONN,
191 Auditorium Road, Storrs, CT 06269, United States
[3] Department of Molecular and Cell Biology, UCONN,
91 North Eagleville Road, Storrs, CT 06269, United States
[4] Department of Medicine, UCONN Health Center,
263 Farmington Avenue, Farmington, CT 06030, United States
[5] Department of Cell Biology, UCONN Health Center,
263 Farmington Avenue, Farmington, CT 06030, United States
[6] Department of Pathology and Laboratory Medicine, UCONN Health Center,
263 Farmington Avenue, Farmington, CT 06030, United States
[7] Connecticut Institute for Clinical and Translational Science,
195 Farmington Avenue, Farmington, CT 06030, United States
[8] Department of Medicine, Endocrinology, UCONN Health Center,
263 Farmington Avenue, Farmington, CT 06030, United States
[9] Institute for Regenerative Engineering, UCONN Health Center,
263 Farmington Avenue, Farmington, CT 06030, United States
[10] Department of Orthopedic Surgery, UCONN Health Center,
263 Farmington Avenue, Farmington, CT 06030, United States
[11] Department of Mechanical Engineering and Applied Mechanics, University of Pennsylvania,
220 South 33rd Street, Philadelphia, PA 19104, United States

*Corresponding Author*: Dr. Thanh D. Nguyen
UCONN, 191 Auditorium Road, 06269, United States
Email: nguyentd@uconn.edu

**Materials and Methods**

*Preparation of PLLA film:*

Poly(L-Lactic acid) (PLLA) granules (PURASORB PL24) used in this work were purchased from Corbion Purac (Amsterdam, the Netherlands). PLLA films with thickness ca. 35 μm were obtained from compression molding using a Carver Laboratory Press (Model 2731, USA) at 200 ºC. PLLA granules were dried at 80 ºC in a vacuum oven overnight prior to compression molding. Rectangle films (ca. 6 cm long and 4.5 cm wide) from compression molding were annealed at 90 ºC for ca. 1 hr and then a series of weights was added to the films to get it stretched. Afterward, the treatment of the films was held at the same temperature for another 7 hours in an oven. Finally, they were quenched and immersed by dry ice for ca. 30 mins to retain the orientation of PLLA chains.

*Fabrication of Non-Biodegradable PLLA sensor*:

*One layer sensor*: Aluminum (Al) foils were used as electrodes to compactly sandwich both surfaces of treated PLLA film (rectangle films with a dimension of 3 cm long, 2 cm wide and 35 μm thick, cutting of films was done in a 45ºangle with the stretching direction). Afterwards, polyimide tape was used as an encapsulation layer to isolate the Al electrodes from air.

*Multilayer PLLA sensors*: The fabrication of sensors is exactly the same as that of one layer ones, but the sandwiched structure was folded in the way shown in a way consistent with Figure 1 (main text).

*Measurements under vibration system*:

The PLLA film sensor (2-layer compression molded PLLA, ca. 3.2 cm long and 2.1 cm wide) was mounted on the surface of the beam (see the schematic in Figure 3a), which was firmly connected to an electrodynamic transducer (ET-132-2, Labworks Inc., California, USA). The transducer was

driven by a power amplifier (PA-151, Labworks Inc., California, USA) with a given voltage and frequency. The voltage was measured using an 8-channel oscilloscope (PicoScope 4000, UK). For the open circuit voltage measurement of PLLA sensors, the input voltage for the power amplifier was fixed at 1V.

*Measurements under impact system*:

PLLA sensors were firmly fixed on the Al beam in the vibration system as shown in the schematic in Figure 3a. To make sure the external force was evenly applied to the sensor, a rigid Al plate was used to cover the sensor. The force applied to the PLLA sensor was measured via a quartz dynamic force sensor (PCB Piezotronics, NY, USA), which was installed on the electrodynamic transducer (ET-132-2, Labworks Inc., California, USA). The input to the transducer was 1V (peak to peak voltage from the function generator).

*Characterization of PLLA film*:

*1-D xrd*: 1-D wide angle x-ray diffraction (WXRD) measurements of PLLA films were carried out at room temperature using a Bruker D2 Phaser (Bruker D2 Phaser, USA). Patterns were recorded from 5ºto 45º with a scan speed of 0.2º/min.

*2-D xrd*: 2-D WAXD was performed on Oxford Diffraction instrument (XCalibur PX Ultra) with an Onyx detector (Cu Kα radiation of 1.542 Å, double mirror focusing, 40 kV and 40 mA) to investigate the orientation of molecule chains after stretching.

*Fabrication of Biodegradable PLLA Sensor*:

*To make the PLLA glue*: acetone and chloroform obtained from Sigma Aldrich were mixed in a 3:1 ratio. Next, PLLA (PURASORB PL24, Corbion Purac) is added and dissolved until the solution becomes viscous. The biodegradable adhesive is used as needed to adhere encapsulating

layers of PLA(Poly-Lactic Acid). Upon use, the sensors are given 24 hours to allow for solvent evaporation.

*To make single-layer sensor*: Treated PLLA with a draw ratio of 4.6 was cut into a 5mm x 5mm film. Two 5mm x 5mm squares attached to 2 mm wide wires were cut out of a 0.05 mm x 100 mm x 100mm sheet of Molybdenum (YiFun Trade, purity 99.96%) using a pair of scissors. The film was sandwiched between the two electrodes, and verification of resistance was done using a multimeter (Extech, MN35). The electrode/film combination was then sandwiched between two 10mm x10mm x 100µm layers of untreated PLLA (PURASORB PL24, Corbion Purac). All of the edges of the encapsulator were then sealed using a combination of the biodegradable PLLA glue and a thermal bag sealer (ULINE, H-161) for 4 seconds. If longer degradation times are desired, PCL, polycaprolactone (PolySciences, Mw: 50,000), can be thermally sealed to the sensor edges to ensure a water tight device.

*To make multi-layer sensor*: Treated PLLA with a draw ratio of 4.6 was cut into a 3mm x 15mm film. 20nm of Iron (Kurt J Lesker, EVMFE35EXEA) and 4µm of Magnesium (Kurt J Lesker, EVMMG35QXQ-A) was then deposited on both sides of the PLLA film using an Electron Beam Evaporator. The film was cut five times, resulting in one electrode surface on the top and the other on the bottom of each patch. Mo wires (ESPI Metal, Knc2040) were then placed against each surface and the electrode/film combination was then sandwiched between two 5mm x 5mm x 100µm layers of untreated PLLA (PURASORB PL24, Corbion Purac). All of the edges of the encapsulator were then sealed using a combination of the biodegradable PLLA glue and a thermal bag sealer (ULINE, H-161) for 4 seconds. If longer degradation times are desired, PCL, polycaprolactone (PolySciences, Mw: 50,000), can be thermally sealed to the sensor edges to ensure a water tight device.

*Characterization and calibration of Biodegradable PLLA Sensor*:

Electrical charge-amplifier circuit shown in Figure S12 was assembled using op amps purchased from Analog Devices (AD8605ARTZ). The biodegradable PLLA sensor was then wired into the circuit and the circuit output was wired to an oscilloscope (PicoScope, 4824) and viewed on a computer. A series of weights (Ohaus, 78023) (sizes 10g, 20, 50g, 100g, 200g, 500g, 700g, 1kg) was then applied to sensor at a frequency of 0.3Hz. The output for each weight cycle was then recorded, and the magnitude of each voltage peak was averaged across three trials. The results were then used to make a calibration plot.

*In vitro experiment*:

*Sensor functionality in vitro*: The sensor was calibrated as previously described. The sensor was then placed in phosphate buffer saline (PBS) at 37˚C for a period of 2 days, where it was removed, rinsed with deionized water, and subjected to the pressures used for its intial calibration. This process was then repeated with the same sensor up to a fully degradation period of 4 days.

*Encapsulator thickness's influence on degradation*: Experiment was performed, following a previous report (see caption of Fig. S17). All of the sensors (n = 4 for each thickness) were initially placed in PBS at 37ºC. As PLA has a long degradation time, over a course of 14-days, there was no significant change in weight for all sensors. In order to illustrate the influence of encapsulator thickness on degradation, the temperature was increased to 74˚C at date 14 to accelerate the sensor erosion.

*In vivo experiment*:

All animal care and procedures were approved by the University of Connecticut School of Medicine Institutional Animal Care and Use Committee (IACUC).

*Measuring the pressure of diaphragmatic contraction*; a multilayer sensor like the one previously described was used for this measurement. The C57BL/6J wild-type mice purchased from The Jackson Laboratory (Stock# 000664) were used for the experiments. The mouse was anesthetized with Ketamine/Xylazine (90-120 mg/kg + 5-10 mg/kg) IP injection. To overdose and euthanize the animals, we doubled this amount of anesthetics. Mice were given Buprenorphine at 1/2 the total dose (0.05-0.1 mg/kg) SQ for pre-operative analgesia. A small 2mm x 8mm incision was made on the shaved abdomen of the mouse. The sensor was then implanted into the mouse and adhered to the bottom of the diaphragm wall using medical glue (Loctite 4013, Henkel) see Figure 5c insert. The wires were then run out of the mouse's abdominal cavity and the incision was closed using the #6 medical suture (Ethilon #230000697G, Owens, MA). The mouse was then allowed to rest fifteen minutes prior to measurement of the diaphragmatic contraction pressure. The wires were then connected to the circuit shown in Figure S12 and the circuit output was connected to an oscilloscope (PicoScope, 4824) and the signals were monitored on a computer. Using the calibration plot generated for this sensor, we determined the force the sensor experienced.

*Assessing sensor functionality after implantation*: Five sensors per time point (date 2, 4, 8 and 16) were calibrated as previously described. The sensor's wires were then encapsulated in PLA, to ensure the device was water tight. The sensors were sterilized by soaking in 200 proof ethanol for 20 minutes, followed by exposure to UV light on both sides of the device for a period of 10 minutes each side. The sensors were then subcutaneously implanted in the backs of mice as seen in Figure S20. The sensors were promptly removed at 2,4,8 and 16 days. The wires for each patch were then exposed and the sensors were recalibrated in the same manner as their initial calibration.

*Statistical analysis of in vivo sensor data*: At each time point, five sensors are subjected to pressures of 4.9, 9.8 and 19.6 kPa. Each pressure is applied three times to the sensors, resulting in

fifteen voltage signals per pressure. The fifteen voltage signals per pressure are averaged together, and plotted along with the calculated standard deviation for the data set as depicted in Figure S16. We calculate p-values for the data, using a two-tailed t-test assuming unequal variances. The averaged voltage, post implantation, for a given pressure at each time point, is compared to the original averaged voltage (i.e. prior to implantation) for the same pressure from 5 sensors. Using Microsoft Excel 2016, the p-values are calculated and depicted above each data group in Figure S16.

*Implantation for histology analysis*: The PLLA sensors were inserted into a surgically-made pockets underneath of the skin of CD1 mice (Charles River). Antibiotics and analgesics were administered post-operatively. The skin over the incision was closed with 4-0 Vicryl sutures (Ethicon, Inc). At different time points of 14 days and 28 days, the animals will be euthanized and tissues will be extracted, fixed, sliced and stained with Hematoxylin & Eosin (H&E), Masson's trichrome and CD-64 antibody (for specifically staining macrophages) imaged by microscope. All animal procedures are approved and performed following IACUC guidelines.

*Staining procedures and histological analysis*: Tissue samples were immersed in formalin for 3 days, washed with water, and placed in 70% ethanol for storage. For sectioning, samples were embedded in paraffin at room temperature. Embedded sections were cut into 5 μm thick sections and mounted on glass slides. Tissue sections were stained with hematoxylin and eosin (H&E), and Masson Trichrosome. All sections were digitally examined using a DAGE-MTI Magic App microscope software coupled to a DAGE-MTI color camera and an Olympus BH-2 microscope (Olympus Corp).

*Immunohistochemistry*: For the macrophage immunohistochemistry staining, tissue sections were obtained and fixed with formalin for 48 hours at 4°C, deparaffinized in xylene and rehydrated in

ethanol. Non-specific staining was blocked by incubation with 10% normal goat serum block for 20 mins at room temperature. Immuno-staining was performed on sections with anti-CD64 (Sino Biological Inc). Sections were incubated overnight at 4°C (dilution 1:100). Bound antibody was detected with a secondary ImmPRESS ™ HRP- Polymer Anti-rabbit IgG (Vector Laboratories) for 30 mins at room temperature and visualized using diaminobenzidine (DAB) as a chromogenic substrate according to the manufacturer's instructions (IHC WORLD, LLC.). Counterstaining was performed with hematoxylin. Negative-control slides were obtained by omitting the primary antibody. All sections were digitally examined using DAGE-MTI Magic App microscope software coupled to a DAGE-MTI color camera and an Olympus BH-2 microscope (Olympus Corp).

## Mathematical Modeling

Here, we aim to present a mathematical model of the piezoelectric PLLA material that we have used for the force biosensor. Our goal is to derive the constitutive relations of a PLLA piezoelectric to study (1) how different applied stresses and strains (e.g. normal stress and elongation strain) can induce shear piezoelectric outputs, (2) why the rotated PLLA film can produce voltage while non-rotated PLLA film can't, and (3) relationship between the different geometrical parameters, input stress/strain and electrical output to roughly estimate shear-piezoelectric constants from collected experimental results in vibration and impact tests (Fig. 3 in the main text).

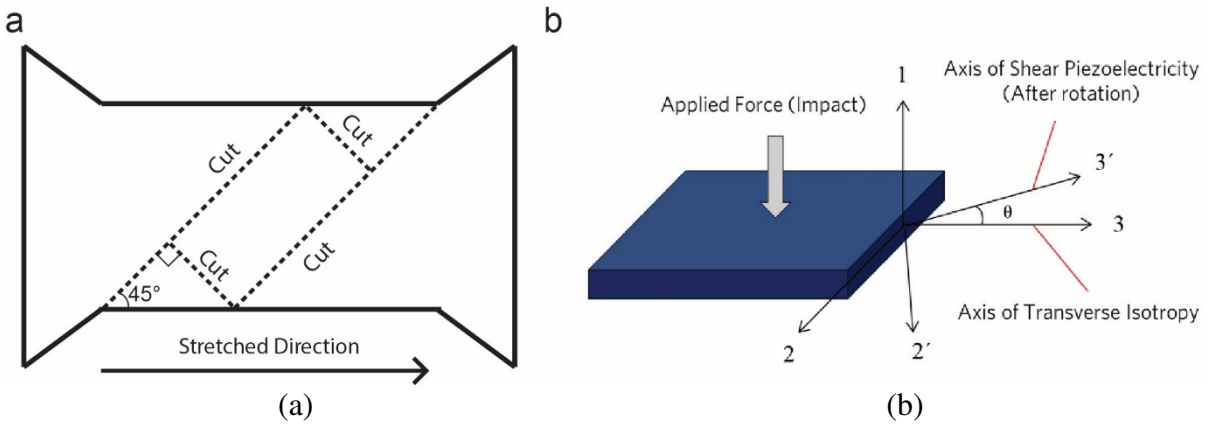


***Figure S1****: a) Simplified schematic of cutting the processed PLLA to transform it into a piezoelectric material. It is important to note that a cutting angle of 45 degrees is utilized for the optimal signal output according to the model derived below. b) Schematic illustrating the direction of the applied force to the treated PLLA films. The axis illustrated in this image are used to derive the model below. Axis 3 is the stretched direction of the film as shown in a).*

- **Direct Piezoelectric Effect (Sensors):**

The direct piezoelectric effect refers to the internal generation of electrical charge resulting from an applied stress or mechanical force. The constitutive relations for the direct effect in a piezoelectric material are (1):

- Tensor notation:

$$\begin{cases} \sigma_{ij} = C_{ijkl}\varepsilon_{kl} - e_{kij}E_k \\ D_i = e_{ikl}\varepsilon_{kl} + X_{ik}E_k \end{cases} \quad (1)$$

This equation shows that an electric displacement and electric field are generated by mechanical stress. The indices *i,j,k,l* can take values 1,2,3.
$\sigma_{ij}$: Stress tensor components [N/m$^2$] (6×1)
$C_{ijkl}$: Stiffness tensor components [N/m$^2$] (6×6)
$\varepsilon_{kl}$: Elastic strain tensor components [dimensionless] (6×1)
$e_{kij}$: Piezoelectric stress tensor components [m/V] or [C/N] (6×3)

$E_k$: Applied electric field components [V/m] (3×1)
$D_i$: Electric displacement vector components [C/m$^2$] (3×1)
$X_{ik}$: Dielectric permittivity components [Farad/m] (3×3)

- Matrix notation (Voigt Notation):

$$\begin{cases} \sigma_p = C_{pq}^{E} \varepsilon_q - e_{pk} E_k \\ D_i = e_{iq} \varepsilon_q + X_{ik}^{\varepsilon} E_k \end{cases} \quad (2)$$

Indices *p,q* take values 1,2,3,4,5,6 and indices *i,k* take values 1,2,3.

- **Inverse (Converse) Piezoelectric Effect (Actuators):**

The inverse piezoelectric effect refers to the internal generation of a mechanical strain resulting from an applied electrical field. The constitutive relations for the inverse effect in a piezoelectric material are (1):

- Tensor notation:

$$\begin{cases} \varepsilon_{ij} = S_{ijkl} \sigma_{kl} + d_{kij} E_k \\ D_i = d_{ikl} \sigma_{kl} + Y_{ik} E_k \end{cases} \quad (3)$$

This equation shows that a piezoelectric material undergoes a deformation under an electric field.
$S_{ijkl}$: Compliance tensor components (inverse of the stiffness matrix) [m$^2$/N] (6×6)
$d_{kij}$: Piezoelectric strain tensor components [m/V] or [C/N] (6×3)
$Y_{ik}$: Dielectric permittivity components [Farad/m] (3×3)

- Matrix notation (Voigt Notation):

$$\begin{cases} \varepsilon_p = S_{pq}^{E} \sigma_q + d_{pk} E_k \\ D_i = d_{iq} \sigma_q + Y_{ik}^{\sigma} E_k \end{cases} \quad (4)$$

- **Relationship between piezoelectric constants:**

The relationship between piezoelectric coefficients are:

$$\begin{aligned} d_{ikl} &= e_{imn} S_{mnkl} \\ e_{ikl} &= d_{imn} C_{mnkl} \end{aligned} \quad (5)$$

Mechanically-stretched PLLA is a special case of anisotropic materials called transversely isotropic. Transversely isotropic materials are those with an axis of symmetry such that any plane perpendicular to this axis is a plane of isotropy. In the case of a transversely isotropic material with axis 3 as the transverse isotropy axis, the number of the independent elastic, piezoelectric and dielectric constants is 5, 3 and 2 respectively (2). In this case, stiffness matrix *C* takes the form (3):

$$C = S^{-1} = \begin{bmatrix} c_{11} & c_{12} & c_{13} & 0 & 0 & 0 \\ c_{12} & c_{11} & c_{13} & 0 & 0 & 0 \\ c_{13} & c_{13} & c_{33} & 0 & 0 & 0 \\ 0 & 0 & 0 & c_{44} & 0 & 0 \\ 0 & 0 & 0 & 0 & c_{44} & 0 \\ 0 & 0 & 0 & 0 & 0 & (c_{11}-c_{12})/2 \end{bmatrix}$$

$$= \begin{bmatrix} 1/Y_p & -\nu_p/Y_p & -\nu_{tp}/Y_t & 0 & 0 & 0 \\ -\nu_p/Y_p & 1/Y_p & -\nu_{tp}/Y_t & 0 & 0 & 0 \\ -\nu_{pt}/Y_p & -\nu_{pt}/Y_p & 1/Y_t & 0 & 0 & 0 \\ 0 & 0 & 0 & 1/2G_t & 0 & 0 \\ 0 & 0 & 0 & 0 & 1/2G_t & 0 \\ 0 & 0 & 0 & 0 & 0 & (1+\nu_p)/Y_p \end{bmatrix}^{-1} \quad (6)$$

*Y*: Young's modulus in 1, 2 and 3 direction
ν: Poisson ratio
*G*: Shear modulus

- **Our model and equations:**

There is only shear piezoelectricity in PLLA, which requires a shear stress as a driving force for the electrical outputs. The piezoelectric strain tensor of the PLLA film is given in previous work (4):

$$d_{ikl} = \begin{bmatrix} 0 & 0 & 0 & d_{14} & 0 & 0 \\ 0 & 0 & 0 & 0 & -d_{14} & 0 \\ 0 & 0 & 0 & 0 & 0 & 0 \end{bmatrix} \quad (7)$$

Here we apply a normal stress ($\sigma_{11}$) that could cause strains and result in an electric field that can be measured as a voltage between two electrodes deposited on two major planes of the PLLA film, along the same 1 direction (Fig. S1b). In order to relate $E_1$ to $\sigma_{11}$ (for sensor) we need to find piezoelectric stress tensor components $e_{kij}$, as seen in equation (1). $e_{kij}$ can be obtained from *d* matrix by using equation (5):

$$e_{kij} = \begin{bmatrix} 0 & 0 & 0 \\ 0 & 0 & 0 \\ 0 & 0 & 0 \\ d_{14}c_{44} & 0 & 0 \\ 0 & -d_{14}c_{44} & 0 \\ 0 & 0 & 0 \end{bmatrix} \quad (8)$$

Using equation (1), the constitutive equations of the PLLA are:

$$\begin{cases} \sigma_{11} = c_{11}\varepsilon_{11} + (c_{11} - 2c_{66})\varepsilon_{22} + c_{13}\varepsilon_{33} \\ \sigma_{22} = (c_{11} - 2c_{66})\varepsilon_{11} + c_{11}\varepsilon_{22} + c_{13}\varepsilon_{33} \\ \sigma_{33} = c_{13}\varepsilon_{11} + c_{13}\varepsilon_{22} + c_{33}\varepsilon_{33} \\ \sigma_{23} = c_{44}\varepsilon_{23} - d_{14}c_{44}E_1 \\ D_1 = d_{14}c_{44}\varepsilon_{23} + \varepsilon_0 X_{11}E_1 \end{cases} \tag{9}$$

Thus, if the axis of transverse isotropy and the axis for shear piezoelectricity coincide, then we cannot get an electric field ($E_1$) in response to the applied stress ($\sigma_{11}$). There will be no electrical response to the applied stress on the same direction, as in the case of $d_{33}$ piezoelectricity. Since PLLA only has shear piezoelectricity, or $d_{14}$, therefore we need to modify the geometry of the PLLA film to induce the driven shear force/strain.

To illustrate this point, we will try to determine how the equations (10) will look when the two axes (transverse isotropy and shear piezoelectricity) are misaligned by $\theta$ by cutting a rectangular PLLA film, at $\theta$ degree relative to the axis of stretching (i.e. axis of transverse isotropy). We will rotate the $e_{kij}$ tensor to account for this rotation.

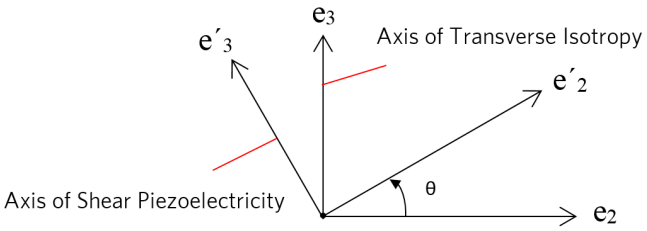


***Figure S2**: Rotated coordinate system through a counterclockwise angle $\theta$*

Considering $c = cos(\theta)$ and $s = sin(\theta)$, we have:

$$\begin{bmatrix} D_1 & D_2 & D_3 \end{bmatrix} = \underbrace{\begin{bmatrix} 1 & 0 & 0 \\ 0 & c & s \\ 0 & -s & c \end{bmatrix}}_{R_3} \begin{bmatrix} D_1' \\ D_2' \\ D_3' \end{bmatrix} \tag{10}$$

For the strain, we have,

$$\begin{bmatrix} \varepsilon_{11} \\ \varepsilon_{22} \\ \varepsilon_{33} \\ \varepsilon_{44} \\ \varepsilon_{55} \\ \varepsilon_{66} \end{bmatrix} = \underbrace{\begin{bmatrix} 1 & 0 & 0 & 0 & 0 & 0 \\ 0 & c^2 & s^2 & cs & 0 & 0 \\ 0 & s^2 & c^2 & -cs & 0 & 0 \\ 0 & cs & -cs & c^2 - s^2 & 0 & 0 \\ 0 & 0 & 0 & 0 & c & c \\ 0 & 0 & 0 & 0 & -s & s \end{bmatrix}}_{R_6} \begin{bmatrix} \varepsilon_{11}' \\ \varepsilon_{22}' \\ \varepsilon_{33}' \\ \varepsilon_{44}' \\ \varepsilon_{55}' \\ \varepsilon_{66}' \end{bmatrix} \tag{11}$$

From equation (1) in the absence of any electric field:

$$D' = e'\varepsilon' \tag{12}$$

or

$$D = R_3 e' R_6^{-1} \varepsilon \tag{13}$$

So,

$$e = R_3 e' R_6^{-1} \tag{14}$$

We can carry out this calculation now and find $e'_{kij}$ as:

$$e'_{kij} = \begin{bmatrix} 0 & 0 & 0 \\ -d_{14} csc_{44} & 0 & 0 \\ +d_{14} csc_{44} & 0 & 0 \\ d_{14}\left(c^2 - s^2\right)c_{44} & 0 & 0 \\ 0 & -d_{14}c^2 c_{44} & +d_{14} csc_{44} \\ 0 & +d_{14} csc_{44} & -d_{14}s^2 c_{44} \end{bmatrix} \tag{15}$$

After rotation, we have these five equations:

$$\begin{cases} \sigma_{11} = c_{11}\varepsilon_{11} + (c_{11} - 2c_{66})\varepsilon_{22} + c_{13}\varepsilon_{33} \\ \sigma_{22} = (c_{11} - 2c_{66})\varepsilon_{11} + c_{11}\varepsilon_{22} + c_{13}\varepsilon_{33} - d_{14}c_{44}E_1 \sin\theta\cos\theta \\ \sigma_{33} = c_{13}\varepsilon_{11} + c_{13}\varepsilon_{22} + c_{33}\varepsilon_{33} + d_{14}c_{44}E_1 \sin\theta\cos\theta \\ \sigma_{23} = c_{44}\varepsilon_{23} - d_{14}\left(\cos^2\theta - \sin^2\theta\right)c_{44}E_1 \\ D_1 = -d_{14}c_{44}\sin\theta\cos\theta\varepsilon_{22} + d_{14}c_{44}\sin\theta\cos\theta\varepsilon_{33} + d_{14}\left(\cos^2\theta - \sin^2\theta\right)c_{44}\varepsilon_{23} + \varepsilon_0 X_{11}E_1 \end{cases} \tag{16}$$

In general, now we expect that if $\sigma_{11} = -P$, then we can get a non-zero $E_1$ as part of solution, when $\theta \neq 0$. If $\theta = 0$, the last equation of (16) will show that $E_1$ or $D_1$ will be 0 under any applied stress $\sigma_{11}$. (Note that $E_1$ and $D_1$ cannot be measured simultaneously. When measuring the output voltage, we need a charge flow through a meter and therefore $E_1 \neq 0$ when and only when $D_1 = 0$ and vice versa).

The values of stiffness matrix depend on the production method of the PLLA film, elongation ratio, molecular weight, optical purity, and crystallinity of the film. Here we used $E$=0.96 [GPa], $E_z$=3.1 [GPa], $\nu_z$=0.3, $\nu$=0.4 and $G_z$=1.0 [GPa] which are similar to the data provided in (5, 6), for a rough calculation.

- **Results:**

**<u>For Impact Mode</u>**

Our results show a linear relation between the applied stress and the generated electric field, and a consistency of experimental data with modeling trend

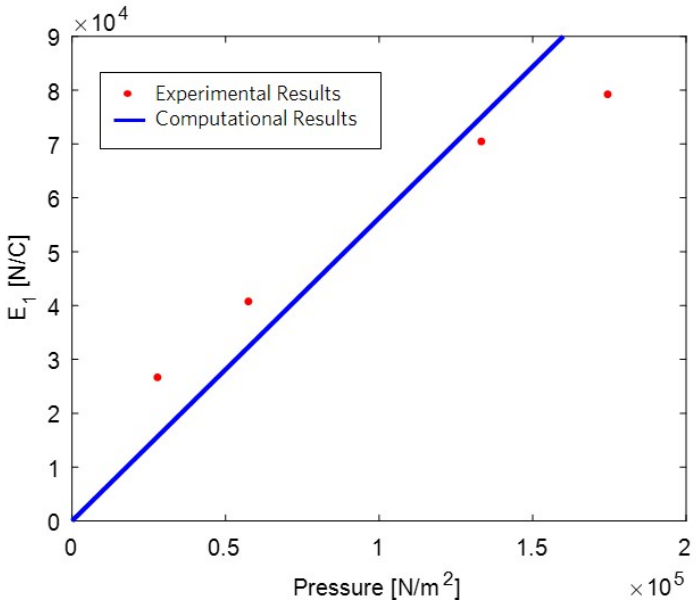


***Figure S3**: Comparison between experimental data represented by red dots and computational results represented by the blue solid line*

This relationship enables a rough estimation of shear piezoelectric constant of $d_{14}$=11.25 [pC/N]. The modeling indicates the maximum electric field is at $\theta$ = 45 [deg], as seen in Fig. S4, which is further reinforced by experimental data (see Fig. S5).

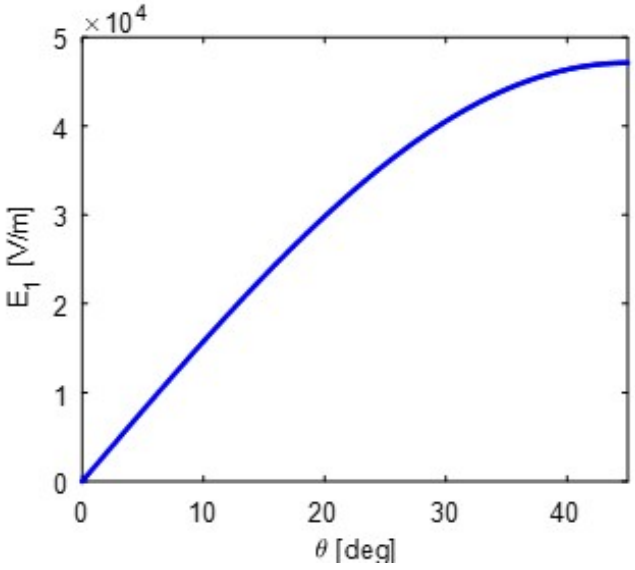


***Figure S4**: Computational results representing effect of different angles on the response of PLLA sensor*

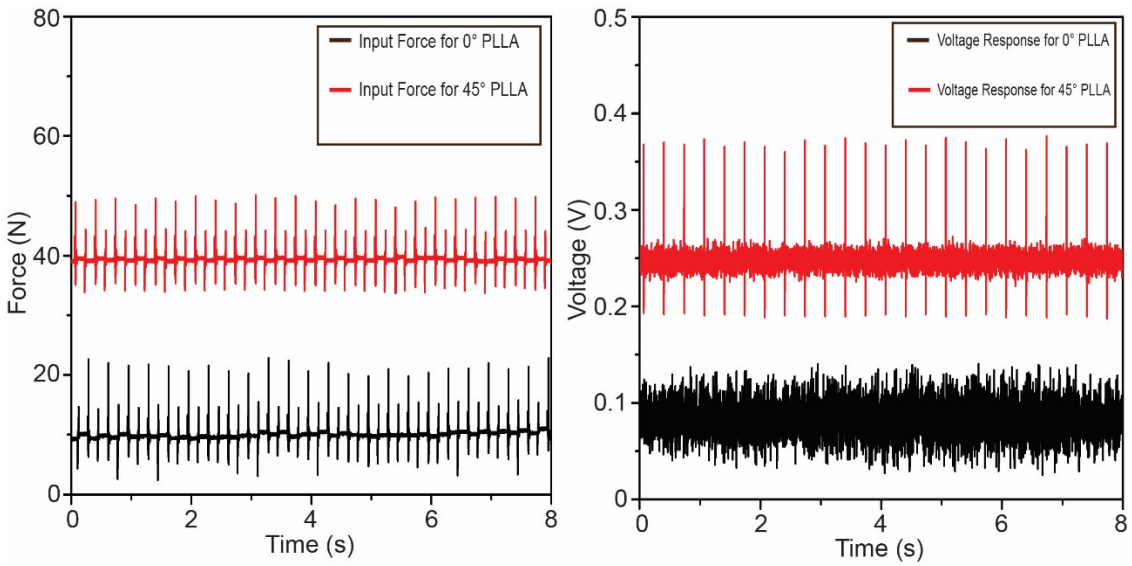


***Figure S5****: Experimental results confirming the accuracy of the theoretical result in Fig. S4; under the same applied impact-force, the treated PLLA (i.e. cut at 45˚) has a clearly defined signal, unlike the PLLA cut at an angle of 0˚, which only has a noise signal.*

**For Vibration Mode**

The inputs are the elongation strain, which is $\varepsilon_{33}$ and the measured output voltage or electrical field $E_1$. Using the same set of equation (16), the PLLA parameters (similar to the impact mode) and experimental data (red points), we again obtain a good fit between experimental and modeling results (Fig. S6) with $d_{14} = 12$ [pC/N]. This result for both impact and vibration modes are in good agreement with(7).

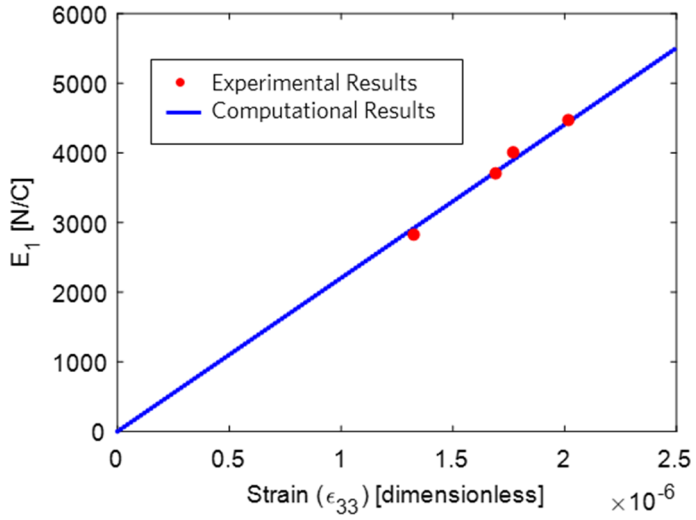


***Figure S6****: Comparison between experimental data represented by red dots and computational results represented by the blue solid line.*

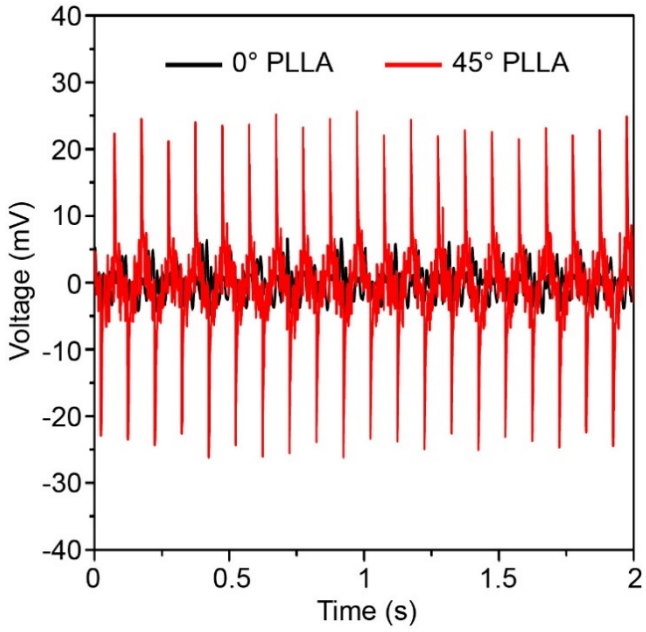


***Figure S7****: Experimental results confirming the accuracy of the theoretical results in Fig. S4 for vibration mode; The samples are subject to a vibration in accordance with the methods described for Figure 3. Similar to the impact mode, under the same applied vibration, the treated PLLA (i.e. cut at 45˚) has a clearly defined signal, unlike the PLLA cut at a 0˚ angle, which only has a noise signal.*

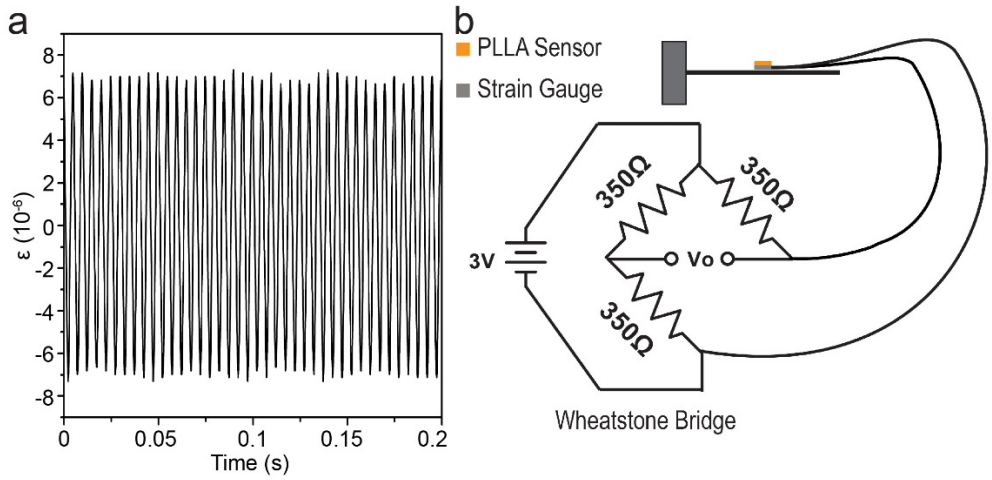


***Figure S8**: **Strain measurement in vibration mode**. a. Strain generated on beam during vibrational characterization of treated PLLA at 200Hz. b. A strain gauge (SGT-3F/350-TY11, OMEGA) is taped to the beam underneath the PLLA sample using Kapton tape. The PLLA sample is then taped above the strain gauge with Kapton tape and the beam is vibrated in accordance with previously described methods. The strain gauge is wired to a balanced Wheatstone bridge and the output voltage from the circuit is run through an instrumentational op amp (INA116PA, Texas Instruments) with a gain of 500. The output voltage is then converted to a strain value through an equation provided by the manufacturer. As can be seen, the measured strain is an oscillating value of about $6x10^{-6}$ strain.*

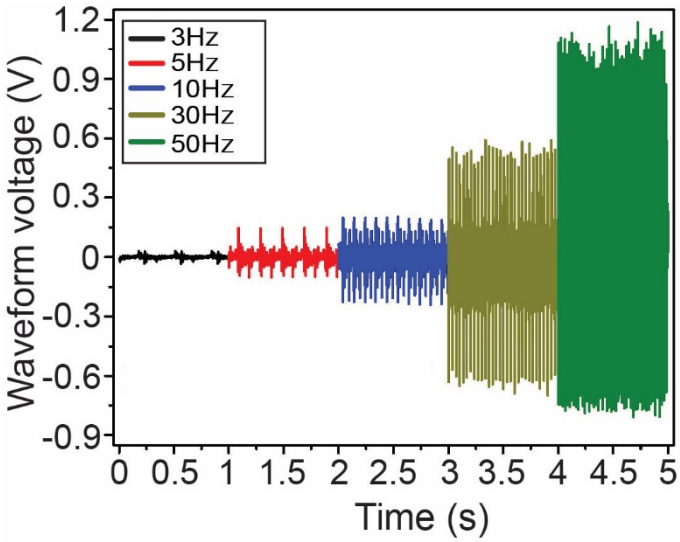


***Figure S9**: **Voltage outputs of a PLLA sensor under applied forces with different frequencies**. A PLLA sensor is affixed to a polycarbonate beam in accordance with the method section described in the main text. In this case the sample is subjected to lower frequency vibrations. At lower frequencies (i.e. 3Hz) the peak to peak voltage output from the PLLA is small (less than 100 mV). However, as the vibration frequency increases to 50Hz, the peak to peak voltage output increases to about 1.6V. Therefore, changing the frequency of the applied vibration clearly changes the signal generated by the PLLA.*

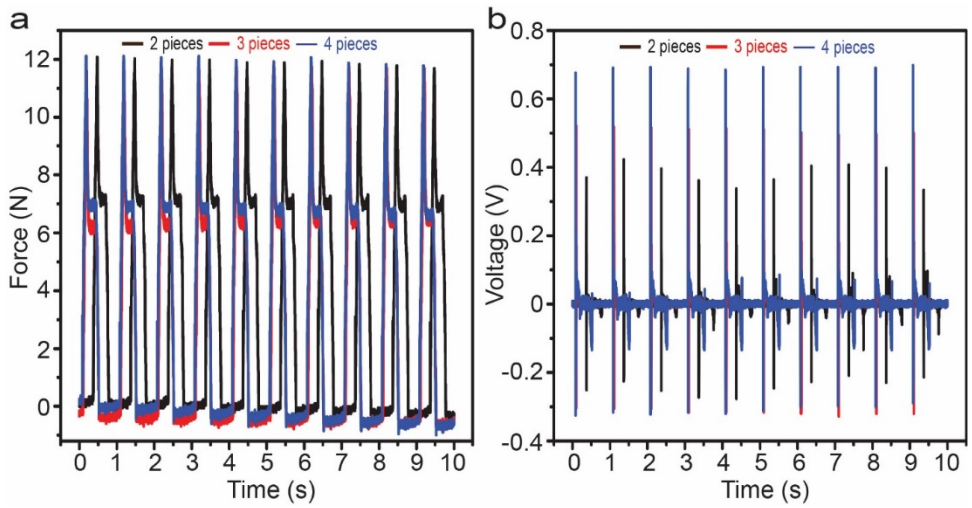


***Figure S10**: **Output voltages, responding to the same applied force, from PLLA sensors made with different numbers of piezoelectric PLLA layers**. a) Force input for sensors fabricated with 2, 3 and 4 layers, and b) The resulting voltage output (measured by an oscilloscope) from the sensors fabricated with different numbers of PLLA layers. It can be seen that increasing the number of layers of PLLA in the sensor increases the voltage output from the sensor under the same applied force. Therefore, sensor sensitivity can be improved through the addition of more layers of PLLA. The samples are subjected to an impact force in accordance with the described methods for Figure 3.*

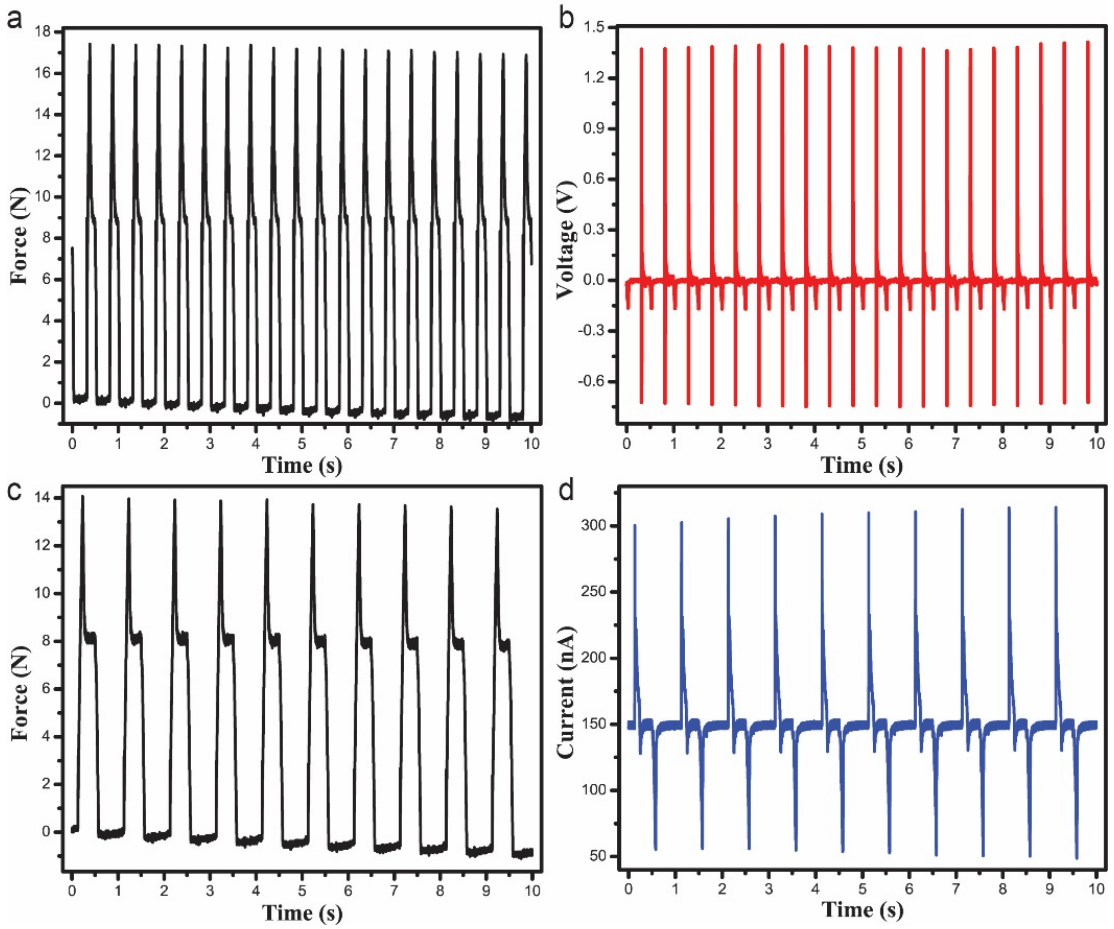


***Figure S11**: **Output piezoelectric voltages and currents of a 6-layer PLLA sensor, responding to applied force**. a) Force input for a PLLA sensor fabricated with 6 layers of treated PLLA with dimensions 1cm x 1cm and b) the resulting voltage output from the multilayer PLLA sensor c) Repeated force input for the 6-layer sensor and d) the resulting current output from the PLLA sensor. All signals were measured by using only an electrometer (Keithley 6514, Tektronix).*

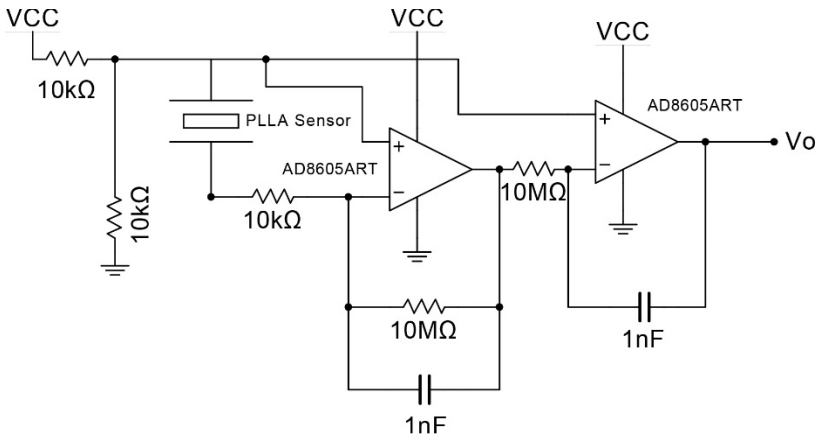


***Figure S12*: Charge amplifier circuit used to measure the charge output from the biodegradable PLLA force sensor.** *$V_{cc}$ represents the voltage input, which in this case is 5 Volts. $V_o$ represents the output voltage from the charge amplifier circuit. A connection between $V_o$ and ground is made using an oscilloscope to measure the output voltage waveform.*

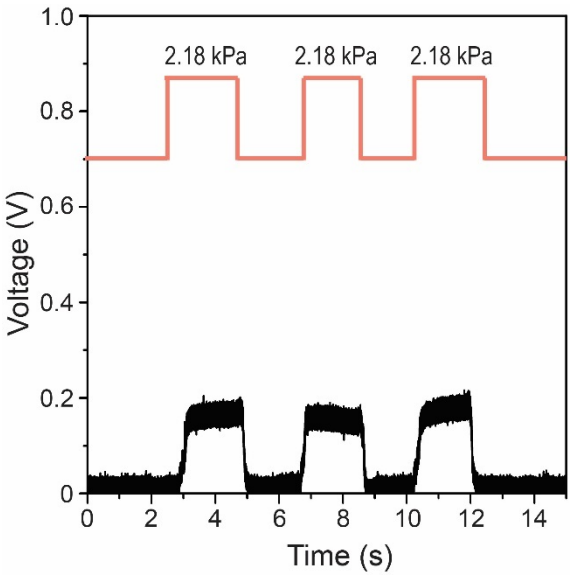


***Figure S13**: **Illustration of consistent signal generated by the same input pressure from the biodegradable sensor**. The red line represents the applied pressure waveform of 2.18 kPa. The black line is the measured voltage signal generated by the biodegradable PLLA force sensor after processing by the charge amplifier circuit illustrated in Figure S12.*

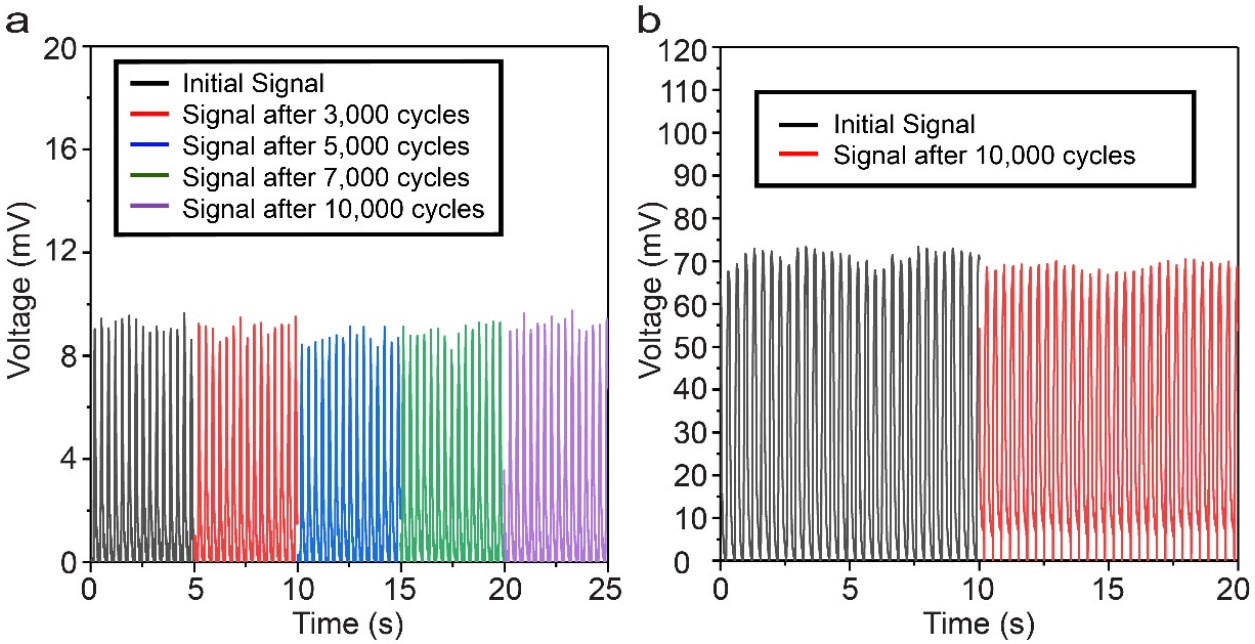


***Figure S14: Reliability of the PLLA sensor over a long measurement period.*** *The sensor was subjected to 10,000 continuous cycles of a 2kPa and 1MPa force at a frequency of 3Hz. a) signal recorded at various stages of the 2kPa cyclic loading testing of the biodegradable force sensor. The signal is consistent throughout the test. b) Signal generated by the biodegradable sensor under an applied cyclic force of 1MPa.*

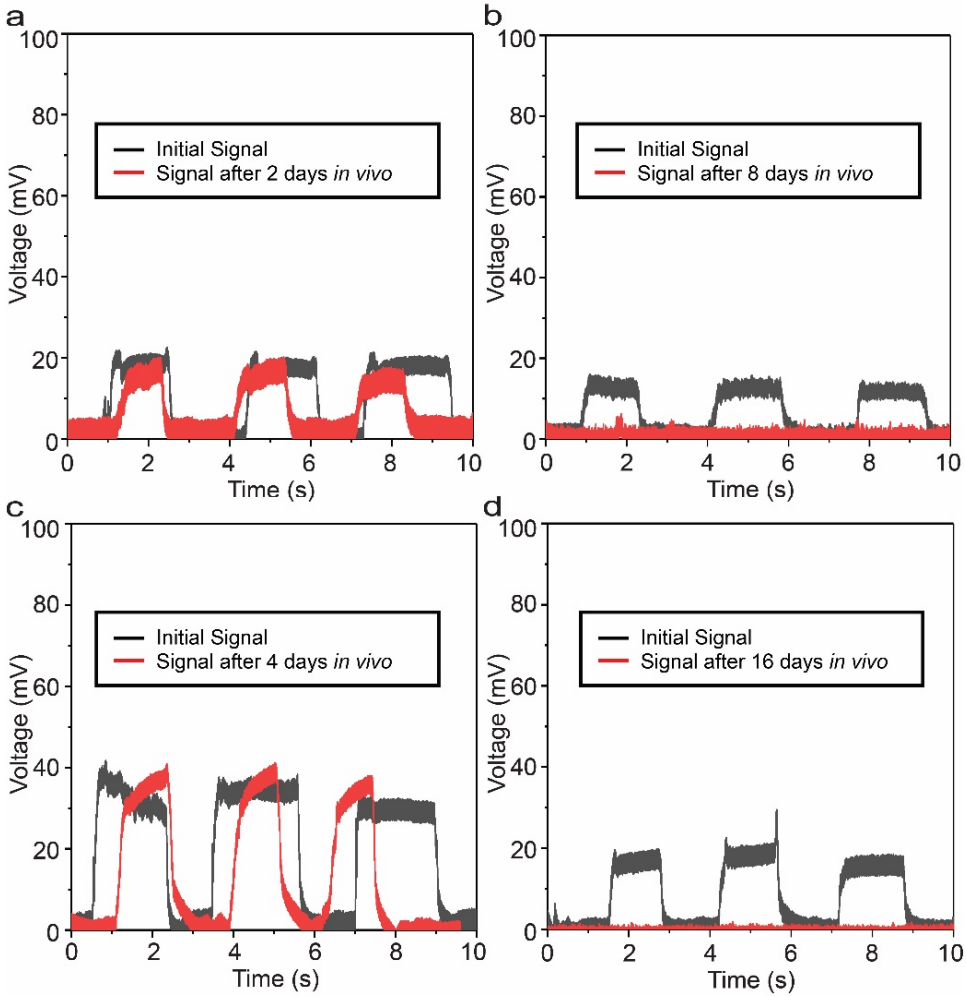


***Figure S15**: **Representative output signals of our PLLA sensors, responding to the same applied pressure, before and after implantation.** The same sensor design, characterized in Fig. 4c of main text, was implanted subcutaneously into the backs of mice (Figure S20) and taken out after 2, 4, 8 and 16 days for recalibration to characterize the device's degradation in vivo and its performance after implantation. a) and c) are comparisons of the signal acquired at date 0 (before implantation) and after implantation periods of 2 and 4 days respectively. b) and d) represent signal loss from the sensor after being implanted for a period of 8 and 16 days respectively. All of the signals shown above are generated under an applied pressure of 4.9kPa. This data shows a similarity between in vitro and in vivo degradation results; a functional lifetime of at least four days is confirmed for both of the studies.*

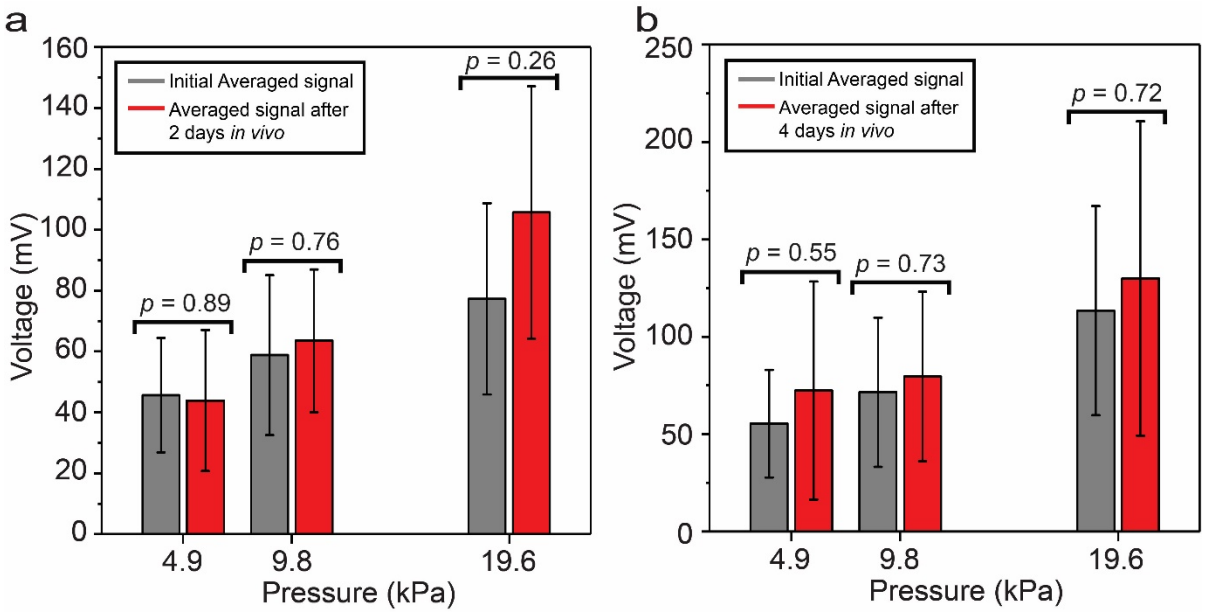


***Figure S16**: **Comparison of output signals from <u>multiple sensors</u>, responding to the same applied pressures, before and after implantation**. a) and b) show this comparison for the sensor output signals, responded to three different applied pressures, before and after 2 and 4 days of implantation, respectively. As described in the caption of Fig. S15, the PLLA sensors were implanted subcutaneously into the backs of mice (Figure S20) and taken out at four different time points of 2, 4, 8 and 16 days after implantation for re-characterizing the devices' performance. There are five sensors per degradation time point, or 20 sensors in total that were used for statistical comparison. At each time point, 5 sensors are subjected to pressures of 4.9, 9.8 and 19.6 kPa. Each pressure is applied three times to the sensors, resulting in fifteen voltage signals per pressure. The voltage signals per pressure are averaged together along with the calculated standard deviation (SD) from the 5 different sensors. The difference in output voltages of different sensors, responded to the same applied force, is normal as each fabricated device requires its own calibration curve, similar to commercial sensors. We calculated p-values for the data, using a two-tailed t-test assuming unequal variances. The averaged voltage, post implantation, for a given pressure at each time point, was compared to the original averaged voltage (i.e. prior to implantation) for the same pressure from the 5 sensors. Using Microsoft Excel 2016, the two-tailed p-values were calculated. Since all of the p-values are greater than the significance level of 0.05, there is no evidence to conclude that the mean voltage signal significantly differs before and after implantation. This assures the usability of the sensors for up to a period of 4 days in vivo. The sensors implanted for 8 and 16 days no longer function as seen in Fig. S15b and S15d.*

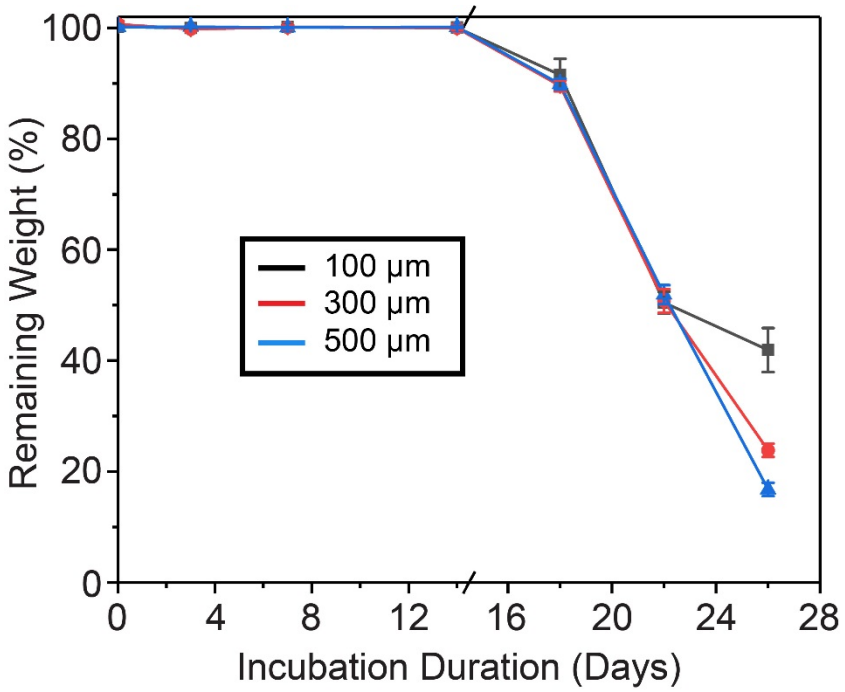


***Figure S17*: Remaining weight (%) of the biodegradable sensors with different thicknesses of PLA encapsulating layers in PBS (phosphate buffered saline) solution over time**. *Experiment was performed, following a previous report (8). All of the sensors (n = 4 for each thickness) were initially placed in PBS at 37°C. As PLA has a long degradation time, over a course of 14-days, there was no significant change in weight for all sensors. In order to illustrate the influence of encapsulator thickness on degradation, the temperature was increased to 74˚C at date 14 to accelerate the sensor erosion. It can be seen that with increasing thickness of PLA encapsulating layers, the sensors exhibit larger mass loss due to the bulk erosion of PLA, which is consistent with reported works (9, 10). While this is the result of an accelerated degradation, the trend should hold for degradation studies performed over a longer period of time at 37 ˚C.*

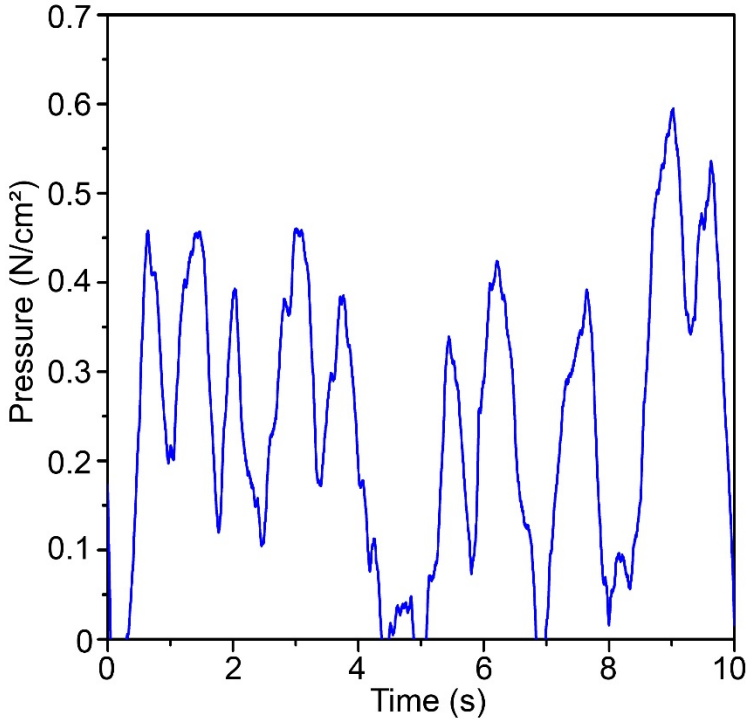


***Figure S18**: **Pressure signal acquired from mouse after overdose of anesthesia, right before the animal's death** (see Fig. 5c in main text). Right before the death, the animal performed atypical heavy breathing with a four-fold increase in the pressure generated by diaphragmatic contractions, likely due to higher amounts of oxygen being inhaled, and less breathing frequency. This breathing pattern is consistent with many reports on "agonal" respiration in mice.(11, 12) The PLLA sensor could therefore be used as a means to detect breathing disorder and other pulmonary diseases.(13)*

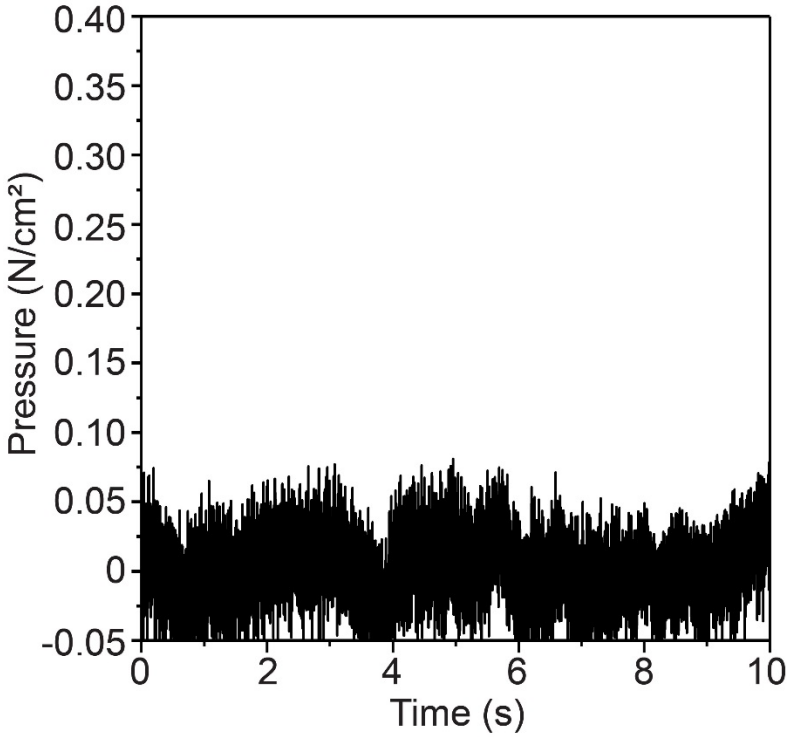


***Figure S19**: **Signal acquired from a biodegradable <u>non-treated</u> PLLA sensor**, implanted into a mouse abdomen for measuring pressure generated by diaphragmatic contractions. The experiment was done exactly the same as the one in Fig. 5c of the main text and the sensor was also made with the same design and materials, except for the non-treated PLLA. As seen in the image, the signals are purely noise (for both cases when the animal was alive and euthanized) with no consistent frequency or magnitude, compared to data in Fig. 5c of the main text.*

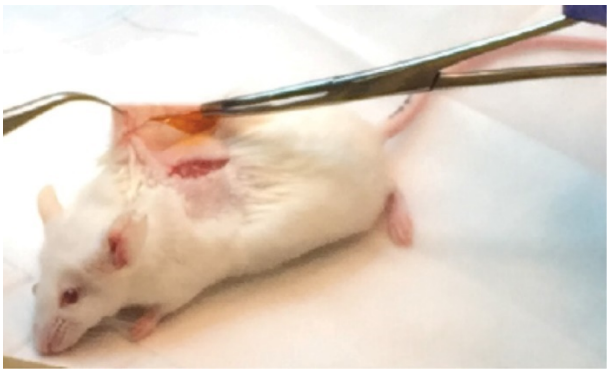

***Figure S20**: **Subcutaneous implantation**. Sensors were implanted into the backs of mice subcutaneously as shown in the image above for the in vivo degradation study and histological analysis. Depending on the size of mice, each mouse receives one or two samples. The wound is then sutured shut until the device's removal. At the time of removal, all mice are euthanized in accordance with IACUC protocols.*

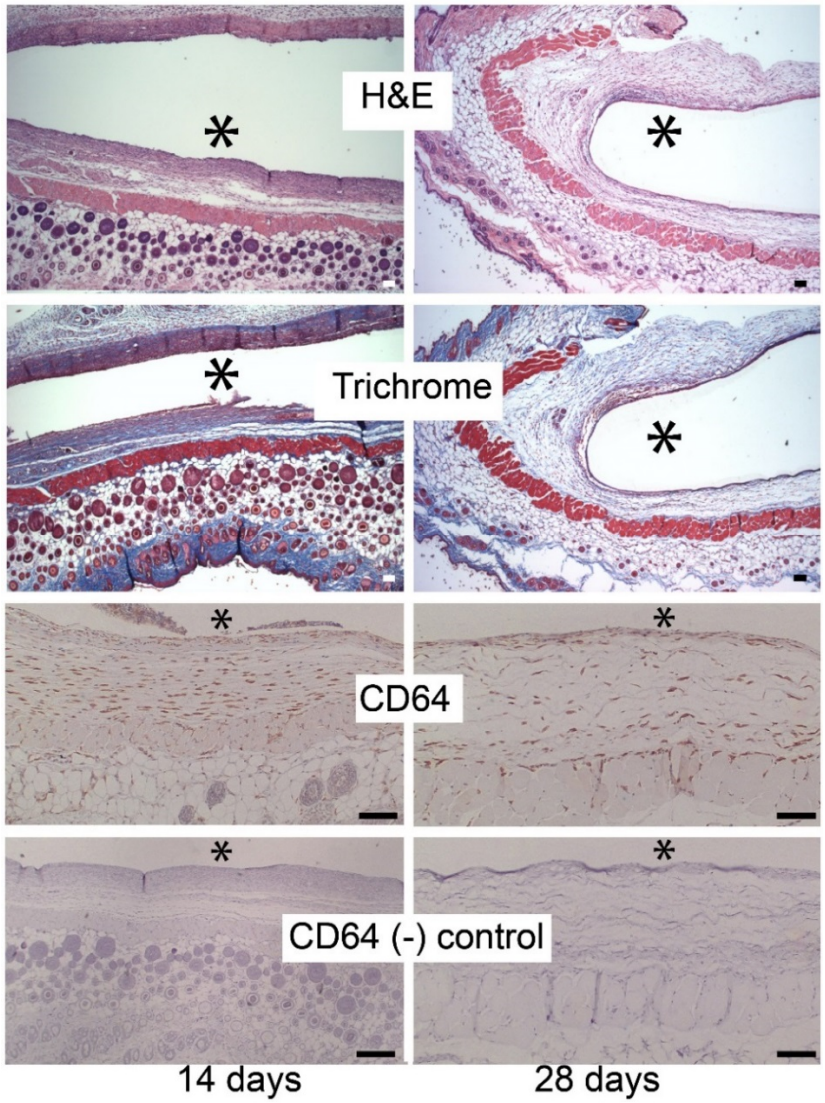


***Figure S21*: Representative histology images (stained with H&E, Thrichome Masson and CD64 antibody) for the biodegradable PLLA sensors after 14 and 28 days of implantation (6 devices for each time point).** *These images are in addition to Fig. 5d-g in the main text. Asterisks (*) show locations of the implanted devices. H&E (Hematoxylin & Eosin) (1st row) is a common stain for imflammatory cells. Masson's trichrome blue (2nd row) is used to demonstrate fibrosis because Masson's trichrome stains collagen, a main component of fibrosis. The collagen is stained blue while skeletal muscle, vessels and epithelium are stained red. Immunohistochemical stains for CD64 (3rd row) are used to reveal macrophages. Positive results are shown in brown color. The specificity of the immunostaining is confirmed by appropriate negative control (omitted primary antibody, as seen in the 4th-row images) and internal negative control (unstained muscles, vessels and hair follicles in the same 3rd-row images). All scale bars are 100 μm. The histological images show only a mild immune reaction without significant presence of inflammation, multi-nucleated giant cells and fibrous capsules. Mild fibrosis and activated macrophages are seen at 2 weeks, but remarkably reduced to normal level at 4 weeks. This is also consistent with what is observed for subcutaneous implantion of PLGA (or PLA-based) microparticles.(14)*

| Material / Device | Young's Modulus |
|---|---|
| PLA Encapsulator | 1.5 GPa |
| Piezoelectric PLLA | 5.0 GPa |
| Molybdenum | 300 GPa (15) |
| Sensor | 340 GPa |

***Table S1**: **Table summarizing the Young's Modulus for the materials present in the sensor as well as a fully assembled sensor**. The Young's Modulus of the PLA encapsulator and piezoelectric PLLA are suitable for integration with bone tissue (16). Despite such a large modulus, the PLLA sensor can be also made into an ultrathin structures with a small bending modulus, allowing the device to be extremely flexible and easy to be integrated with soft tissues (e.g. skin and brain), similar to many other reported bio-integrated flexible electronics made of hard and stiff electronic materials. (17).*

| Draw Ratio | Herman's Orientation Function |
|---|---|
| 1 | 0 |
| 2.5 | 0.5 |
| 4.6 | 0.89 |
| 6.5 | 0.81 |

***Table S2**: **Table summarizing the calculated Herman's Orientation Function for different draw ratios of treated PLLA**. These values were derived along with the 2D WAXS results illustrated in Figure 2 (main text) using software (CrysAlis$^{Pro}$ v.38.49, Rigaku, and AAnalyzer, RDATAA) in conjunction with the XCalibur PX Ultra (Rigaku Oxford Diffraction). The software calculates how close the 2D XRD signals are to the axis of interest. As the films become more oriented, the signal changes from an amorphous circle to a band. The less the signal band deviates from the stretched axis, the more oriented the film is. A value of 0 indicates a completely amorphous film, while a value of 1 indicates a perfectly oriented film along the stretching direction. As can be seen from the table, the orientation degree increases up to 0.89 for a film of draw ratio 4.6. However, exceeding this draw ratio appears to result in a decreased orientation degree. This agrees with the 1D XRD data obtained in Figure 2.*

**References:**


1. Tiersten HF (2013) *Linear Piezoelectric Plate Vibrations: Elements of the Linear Theory of Piezoelectricity and the Vibrations Piezoelectric Plates* (Springer).
2. Dineva PS, Gross D, Müller R, & Rangelov T (2014) *Dynamic fracture of piezoelectric materials: solution of time-harmonic problems via BIEM* (Springer Science & Business Media).
3. Bower AF (2009) *Applied mechanics of solids* (CRC press).
4. Ando M, Kawamura H, Kageyama K, & Tajitsu Y (2012) Film sensor device fabricated by a piezoelectric poly (l-lactic acid) film. *Japanese Journal of Applied Physics* 51(9S1):09LD14.
5. Jamshidian M, Tehrany EA, Imran M, Jacquot M, & Desobry S (2010) Poly‐Lactic Acid: production, applications, nanocomposites, and release studies. *Comprehensive Reviews in Food Science and Food Safety* 9(5):552-571.
6. Nakagawa T, Nakiri T, Hosoya R, & Tajitsu Y (2004) Electrical properties of biodegradable polylactic acid film. *IEEE Transactions on Industry Applications* 40(4):1020-1024.
7. Ochiai T & Fukada E (1998) Electromechanical properties of poly-l-lactic acid. *Japanese journal of applied physics* 37(6R):3374.
8. Boutry CM*, et al.* (2015) A Sensitive and Biodegradable Pressure Sensor Array for Cardiovascular Monitoring. *Adv. Mater.* 27(43):6954-6961.
9. Grayson ACR, Cima MJ, & Langer R (2005) Size and temperature effects on poly (lactic-co-glycolic acid) degradation and microreservoir device performance. *Biomaterials* 26(14):2137-2145.
10. Lu L, Garcia CA, & Mikos AG (1999) In vitro degradation of thin poly (DL‐lactic‐co‐glycolic acid) films. *J. biomed. mater. res., Part A* 46(2):236-244.
11. Ewald AJ, Werb Z, & Egeblad M (2011) Monitoring of Vital Signs for Long-Term Survival of Mice under Anesthesia. *Cold Spring Harb. Protoc.* 2011(2):pdb.prot5563-pdb.prot5563.
12. Jaber SM*, et al.* (2014) Dose Regimens, Variability, and Complications Associated with Using Repeat-Bolus Dosing to Extend a Surgical Plane of Anesthesia in Laboratory Mice. *Journal of the American Association for Laboratory Animal Science : JAALAS* 53(6):684-691.
13. Sinderby C*, et al.* (2001) Diaphragm activation during exercise in chronic obstructive pulmonary disease. *Am. J. Respir. Crit. Care Med.* 163(7):1637-1641.
14. McHugh KJ*, et al.* (2017) Fabrication of fillable microparticles and other complex 3D microstructures. *Science* 357(6356):1138-1142.
15. Dickinson JM & Armstrong PE (1967) Temperature Dependence of the Elastic Constants of Molybdenum. *J. Appl. Phys.* 38(2):602-606.
16. Rho JY, Ashman RB, & Turner CH (1993) Young's modulus of trabecular and cortical bone material: Ultrasonic and microtensile measurements. *J. Biomech.* 26(2):111-119.
17. Rogers JA, Someya T, & Huang Y (2010) Materials and Mechanics for Stretchable Electronics. *Science* 327(5973):1603-1607.